INTERNATIONAL JOURNAL FOR NUMERICAL AND ANALYTICAL METHODS IN GEOMECHANICS, VOL. 5, 229-245 (1981)

NON-LINEAR ANALYSIS OF A JOINT ELEMENT AND ITS APPLICATION IN ROCK ENGINEERING

GE XIURUN (KE HSU-JUN)†
Institute of Rock and Soil Mechanics, Academia Sinica, Wuhan, China

SUMMARY

In this paper models are given for analysis and description of non-linear properties of joints, weak intercalations and interfaces in rock masses.

Models for analysis consist of four parts, i.e. shear displacement model, normal deformation model, shear strength model and a relationship between unit shear stiffness and normal stress.

The method of non-linear analysis given in this paper is based on an incremental procedure.

The proposed method is available for different types of shear-displacement curves, and also adapted to the complicated process of loading–unloading–reloading.

The results of computer simulation of an *in-situ* shear test obtained by this method gave a good fit to the measured data.

The method of non-linear analysis of joint elements has been used in some practical rock engineering problems, and some interesting results and conclusions have been obtained.

MODELS AND METHOD FOR NON-LINEAR ANALYSIS OF JOINT ELEMENT

The non-linear mechanical properties of weak structural planes such as weak intercalations, joints pre-existing in rock masses, and their distribution and combination are in close relation to the deformation and failure of rock masses. So it is important to simulate the non-linear properties in calculation.

Goodman firstly suggested the joint element[1] and gave not only the description of non-linear properties of joints,[2] but also the method of analysis.[3] The iterative procedure is the basis of his method. Clough and Duncan[4] described the non-linear shear–displacement curve as hyperbolic. It is seen that such method is rather difficult to apply, if the curve has an evident stress drop. Some other methods can be found in References 5–7.

Goodman's joint element has been adopted by us, but we suggested the models for non-linear analysis and gave the method of analysis.[8]

Because the incremental analysis is able to give full illustration of the loading process and has obvious advantages in describing complicated process such as loading–unloading–reloading and so on, we apply it as a basic method of analysis for non-linear properties of joint elements. In order to treat the problems of tension failure of a joint element, the stress drop of the shear displacement curve during shear failure and the difference between the peak and residual shear strength of the joint, we use the stress transfer method to make an approximate analysis. In many cases taking such a simplification, i.e. using the stress drop instead of the concrete form of the strain softening portion of the shear displacement curve of the joint is adopted frequently,

† Associate Professor.

0363-9061/81/030229-17$01.70

Received 28 September 1979
Revised 30 April 1980

therefore the stress transfer method used in analysis in such conditions seems also to be applicable.

In this paper the proposed method will be introduced concisely and attention will be focused on its application in some practical rock engineering problems.

The models suggested for non-linear analysis of a joint element consist of the following four parts:

(a) shear displacement model (Figure 1);
(b) normal deformation model (Figure 2);
(c) shear strength model (Figure 3);
(d) relationship between unit shear stiffness k_s and normal stress of joint element σ. It can be described by the following expression:

$$k_s = k_{s0} - \alpha\left(\frac{|\sigma|}{p_a}\right)^m, \qquad \sigma < 0 \tag{1}$$

where p_a is the atmospheric pressure, the dimension of which is the same as that of σ and $\sigma < 0$; in this paper compressive stress σ will be taken as negative. k_{s0}, α and m can be determined

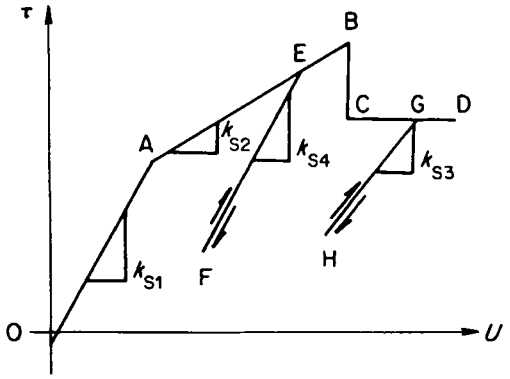

Figure 1. The shear displacement model of joint element

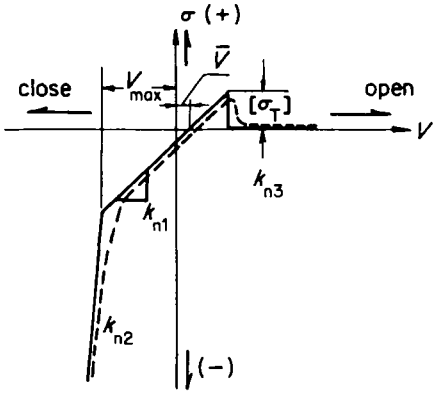

Figure 2. The normal deformation model of joint element

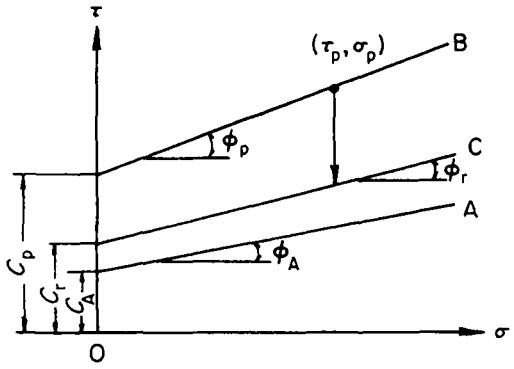

Figure 3. The shear strength model of joint element

according to the family of τ–U curves obtained from experiments. In some cases $m = 1$ can be adopted.

The proposed τ–U model as shown in Figure 1 is quite convenient to simulate any one of the four basic types of shear-displacement curves (Figure 4, (a), (b), (c), (d) obtained from the *in-situ* shear testing.

It is only required to adjust corresponding parameters and there will be sufficient accuracy in application.

$[\sigma_T]$ in the normal deformation model represents the tensile strength of the joint element. If the joint element cannot support tension, $[\sigma_T] = 0$ should be adopted. When $\sigma \geqslant [\sigma_T]$ the joint element not subjected to tension failure is considered to have tension failure occurring, and its stresses drop to zero. The stress transfer method will be used to adjust this portion of stresses dropping to the other elements during tension failure. The $\overline{V}$ shown in Figure 2 is used to identify whether the opened joint element is reclosed. V_{max} is a parameter about ultimate compression.

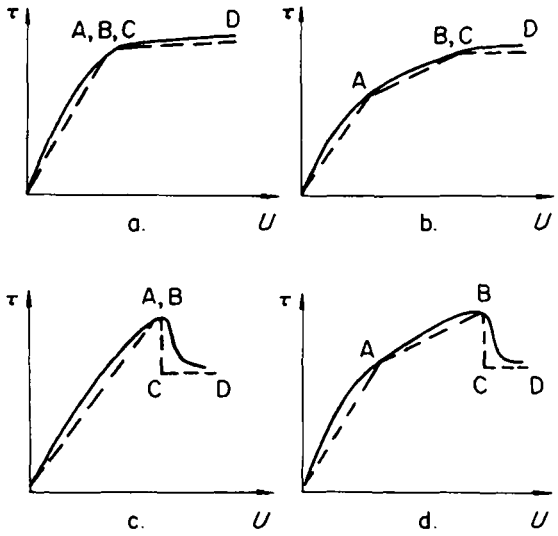

Figure 4. The simulation of the different types of τ–U curve

When $V \leqslant V_{\max}$, the joint element enters into ultimate compression state, then $k_n = k_{n2}$ must be adopted. $k_n = k_{n3} = 0$ is used for the opened joint element, and the reclosed element will be treated as a shear problem, but its tension strength cannot be recovered.

Using the τ–U model of the joint element combined with the shear strength model (Figure 3), we can easily take into account the difference between the peak and residual strengths and the complicated process of loading-unloading–reloading. For example, if $\sigma < 0$ and the following condition is fulfilled,

$$f = |\tau| + \sigma \tan \varphi_p \geqslant C_p \tag{2}$$

the joint element is sheared off to failure. Then its residual stresses τ', σ' should be located on the residual shear strength line. In Figure 3 what is shown is one of the methods of proceeding. The stress transfer method is also used to adjust the stresses which should be relieved. Because the peak shear strength cannot be recovered, so the residual strength will be used as the criterion of the strength and only the k_{s3} can be used as the base for unit shear stiffness for the sheared off joint element.

Before or after point A in the τ–U curve the behaviours of the unsheared off joint element are different. If the point A is passed, the loading or unloading states of the joint element should be distinguished. When the following condition is fulfilled,

$$Q = |\tau| + \sigma \tan \varphi_A - C_A \geqslant 0, \qquad \sigma < 0 \tag{3}$$

this means that the element has reached or exceeded point A of the τ–U curve, otherwise it is in the OA or AO division in Figure 1.

It is required to calculate the value of Q at each stage and to make a comparison between Q and $Q_{\max}$, which has been reached and remembered in its history of loading. When $Q > Q_{\max}$ the element is in the EB division in Figure 1, thus $k_s = k_{s2}$, otherwise the element is in the FE or EF division and $k_s = k_{s4}$.

If the sheared-off joint element is in the state of sliding, we treat this problem as perfect plasticity. Then the equation of mechanical properties of the joint element can be written in incremental form:

$$\begin{Bmatrix} \mathrm{d}\tau \\ \mathrm{d}\sigma \end{Bmatrix} = [C_{ep}] \begin{Bmatrix} \mathrm{d}U \\ \mathrm{d}V \end{Bmatrix} = \begin{bmatrix} k_{ss} & k_{sn} \\ k_{ns} & k_{nn} \end{bmatrix} \begin{Bmatrix} \mathrm{d}U \\ \mathrm{d}V \end{Bmatrix} \tag{4}$$

If the non-associated flow rule is adopted, i.e. the potential surface G and yield surface F are not considered to be coincident $[C_{ep}]$ is

$$[C_{ep}] = \frac{1}{H} \begin{bmatrix} k_s \cdot H - k_s^2 \left(\dfrac{\partial F}{\partial \tau}\right)\left(\dfrac{\partial G}{\partial \tau}\right) & -k_s k_n \left(\dfrac{\partial F}{\partial \sigma}\right)\left(\dfrac{\partial G}{\partial \tau}\right) \\ -k_s k_n \left(\dfrac{\partial F}{\partial \tau}\right)\left(\dfrac{\partial G}{\partial \sigma}\right) & k_n \cdot H - k_n^2 \left(\dfrac{\partial F}{\partial \sigma}\right)\left(\dfrac{\partial G}{\partial \sigma}\right) \end{bmatrix} \tag{5}$$

where

$$H = k_s \left(\frac{\partial F}{\partial \tau}\right)\left(\frac{\partial G}{\partial \tau}\right) + k_n \left(\frac{\partial F}{\partial \sigma}\right)\left(\frac{\partial G}{\partial \sigma}\right) \tag{6}$$

At present, considering the lack of experimental data of the plastic potential surface and non-symmetry of the matrix $[C_{ep}]$, the associated flow rule is used in all of our examples of calculation.

It is required only to use F instead of G in equations (5) and (6).

Function F should be determined from the experiments. It is seen that to take the Coulomb criterion of strength as the concrete form of F is not only simple and convenient but also comparatively in compliance with the practical conditions. Hence F may be written as

$$F = |\tau| + \sigma \tan \varphi_r - C_r = 0, \qquad \sigma < 0 \tag{7}$$

When equation (7) is adopted, the explicit forms of the components of $[C_{ep}]$ are as follows:

$$\left.\begin{aligned} k_{ss} &= \frac{k_{s3} k_n \tan^2 \varphi_r}{H} \\ k_{nn} &= \frac{k_{s3} k_n}{H} \\ k_{sn} = k_{ns} &= \frac{\mp k_{s3} k_n \tan \varphi_r}{H}, \qquad \tau \gtrless 0 \\ H &= k_{s3} + k_n \tan^2 \varphi_r \end{aligned}\right\} \tag{8}$$

The matrix $[C_{ep}]$ is different from the matrix of elastic properties of the joint element $[C]$. The terms of k_{sn} and k_{ns} in the matrix $[C_{ep}]$ mean coupled deformation, and reflect the phenomenon of shear dilatancy to a certain degree.

But not all the sheared-off joint elements are definitely in the state of loading, so we have to derive the criterion of identification of loading and unloading. It may be obtained from the principle of non-negative plastic work. When the following condition is fulfilled,

$$\left.\begin{aligned} |\tau| + \sigma \tan \varphi_r &\geqslant C_r, \qquad \sigma < 0 \\ \text{and} \qquad \\ \mathrm{d}N &\geqslant 0, \end{aligned}\right\} \tag{9}$$

the sheared off joint element is still in the state of loading, otherwise it exists in the state of unloading. The $\mathrm{d}N$ is

$$\mathrm{d}N = k_{s3} \frac{\partial F}{\partial \tau} \mathrm{d}U + k_n \frac{\partial F}{\partial \sigma} \mathrm{d}V \tag{10}$$

where $\mathrm{d}U$, $\mathrm{d}V$ are taken from the results of this stage of calculation. Using equation (10) we can check whether the chosen state of the joint element adopted in the calculation is right.

If the sheared-off joint element is in the state of unloading, instead of $[C_{ep}]$ the matrix $[C]$ will be used.

THE CALCULATION TO SIMULATE THE *IN-SITU* SHEAR TEST

The length of *in-situ* rock specimens is 60 cm. The shearing area, which is located in the thin mud layer within the weak intercalation of argillaceous siltstone, is about 3000 cm^2. The measured family of τ–U curves is shown in Figure 5. This curve can be considered as the type shown in Figure 4(b). The strength parameters obtained from *in-situ* shear tests are as follows: $C_p = C_r = 0{\cdot}32$ kg/cm^2, $\tan \varphi_p = \tan \varphi_r = 0{\cdot}204$, $C_A = 0$, $\tan \varphi_A = 0{\cdot}205$. Based on the measured family of τ–U curves, according to expression (1) we have the deformation parameters when $m = 1$. For the case of k_{s1}: $k_{s0} = 2{\cdot}0$ kg/cm^3, $\alpha = 6{\cdot}0$ kg/cm^3. For the case of k_{s2}: $k_{s0} = 4{\cdot}5$ kg/cm^3,

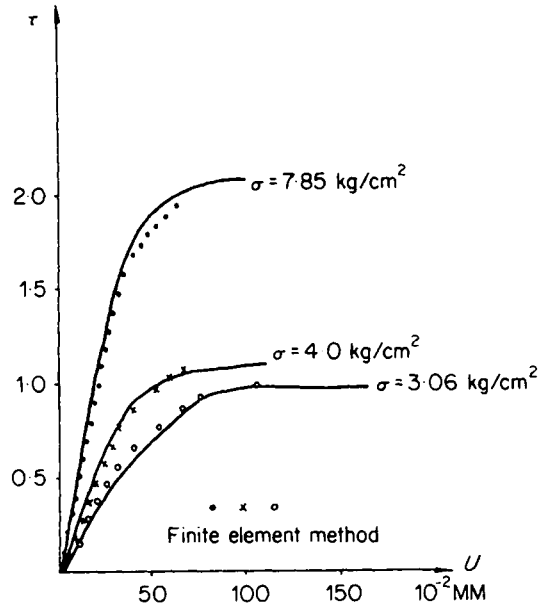

Figure 5. The family of τ–U curves of mudded layer

$\alpha = 0{\cdot}82\ \text{kg/cm}^3$, $k_{n1} = 98{\cdot}0\ \text{kg/cm}^3$, $k_{n3} = 0$. In order to simplify the process we adopted $k_{s1} = k_{s3} = k_{s4}$ and $k_{n1} = k_{n2}$.

The family of τ–U curves of the cemented surface between the concrete and rock has been also measured and is seen in Figure 6. They belong to the type shown in Figure 4 (d). The

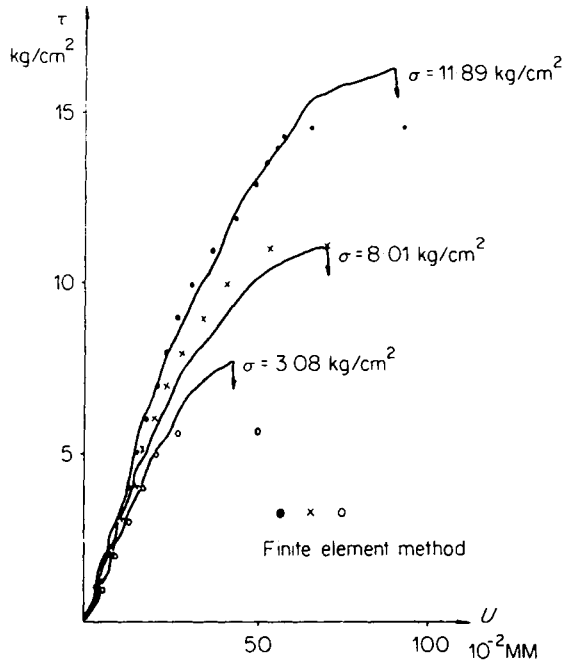

Figure 6. The family of τ–U curves of cemented surface between rock and concrete

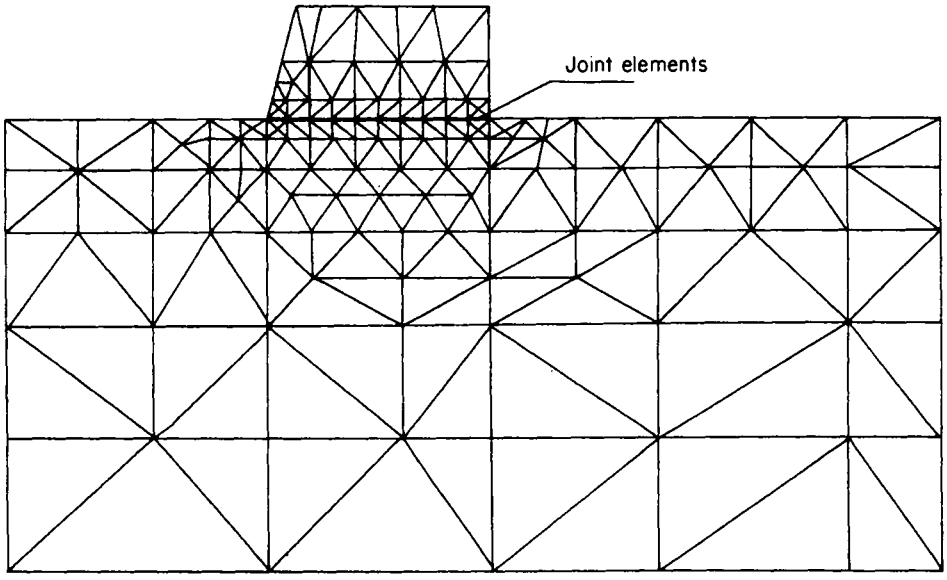

Figure 7. Finite element mesh to simulate the *in-situ* shear test

strength parameters are: $C_p = 3{\cdot}1$ kg/cm^2, tan $\varphi_p = 1{\cdot}1$, $C_r = 1{\cdot}5$ kg/cm^2, tan $\varphi_r = 0{\cdot}81$, $C_A = 4{\cdot}0$ kg/cm^2, tan $\varphi_A = 0{\cdot}54$. When $m = 1$, the deformation parameters are as follows: for the case of k_{s1}: $k_{s0} = 230{\cdot}0$ kg/cm^3, $\alpha = 10{\cdot}0$ kg/cm^3; for the case of k_{s2}: $k_{s0} = 105{\cdot}0$ kg/cm^3, $\alpha = 4{\cdot}3$ kg/cm^3, $k_{n1} = k_{n2} = 1000{\cdot}0$ kg/cm^3, $k_{n3} = 0$.

The mesh used in the calculation is seen in Figure 7.

During calculation, first of all the vertical loads are applied in 5 steps, and then the thrust which is inclined at an angle of 15° to the shearing surface is applied step by step until the specimen is sheared off along the mud layer or shearing surface. The calculated values of the relative sliding amounts at the central portion of the shear surface are given in Figures 5 and 6. The results of finite element analysis are quite in compliance with the measured curves. What Figure 8 shows is the calculated curves to simulate the loading–unloading–reloading process,

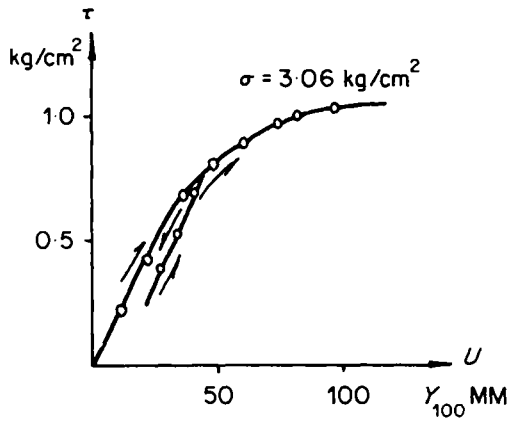

Figure 8. Computation to simulate the process of loading–unloading–reloading

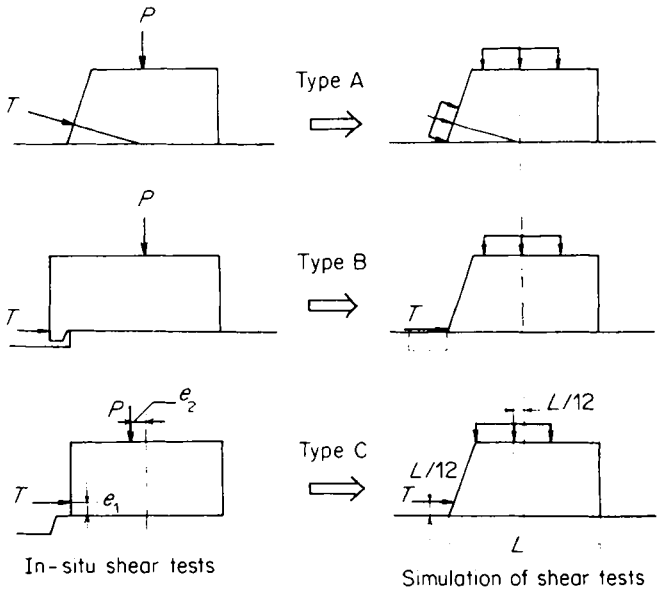

Figure 9. The schemes of different types of shear testing

which is indicated by the arrow. It is seen that the proposed method is available to simulate the complicated process of loading.

THE NUMERICAL ANALYSIS OF THE STRESS DISTRIBUTION OF THREE COMMON USED TYPES OF THE SHEAR TESTS *IN SITU*

The *in-situ* shear test of rock masses, weak planes or cemented surface between the concrete and rock can be done in different ways. What Figure 9 shows are the currently adopted three types of *in-situ* shear test, and we call them Type A, Type B and Type C for simplification. The calculations to simulate the different types of testing have been done in order to know the relation between the stress distribution along the shearing plane and the type of testing used, and to make some comments about them. But the stress distribution is also in close relation to the properties of shearing surface, rock specimens and the situation of their combination. Therefore the calculations to simulate the Types A, B, C of testing have been accomplished for four cases of combination shown in Figure 10.

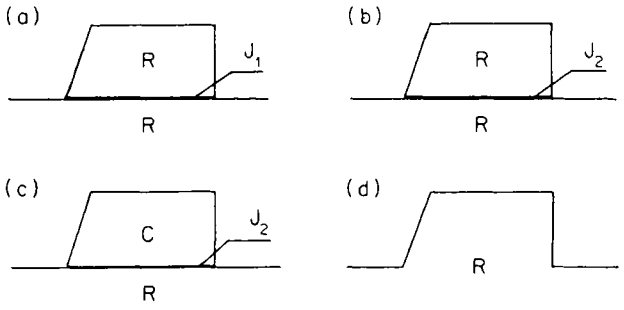

Figure 10. The four types of combination of rock specimens used in the simulation

R and C in Figure 10 represent rock and concrete respectively. Also J_1 in Figure 10 (a) represents the quite weak intercalation or mud layer in rock. The mechanical properties of J_1 are the same as those indicated in Figure 5. J_2 in Figure 10(b) represents joints, but it is also used as the cemented surface between the rock and concrete in Figure 10(c). The family of τ–U curves shown in Figure 6 has also been employed for characterizing the mechanical properties of J_2. Poisson's ratio ν of the rock is 0·3, and its Young's modulus E is 16,000 kg/cm^2, which is much lower than the modulus of concrete.

Figure 10(d) is to simulate the *in-situ* shear test on rock specimens without any weak plane. For brevity we have only to give the distribution of τ and σ along the shearing surface when the average stresses $\bar{\tau}$ and $\bar{\sigma}$ of the surface are equal to some values. Figures 11, 12, 13 and 14 correspond to the cases indicated in Figures 10(a), 10(b), 10(c) and 10(d).

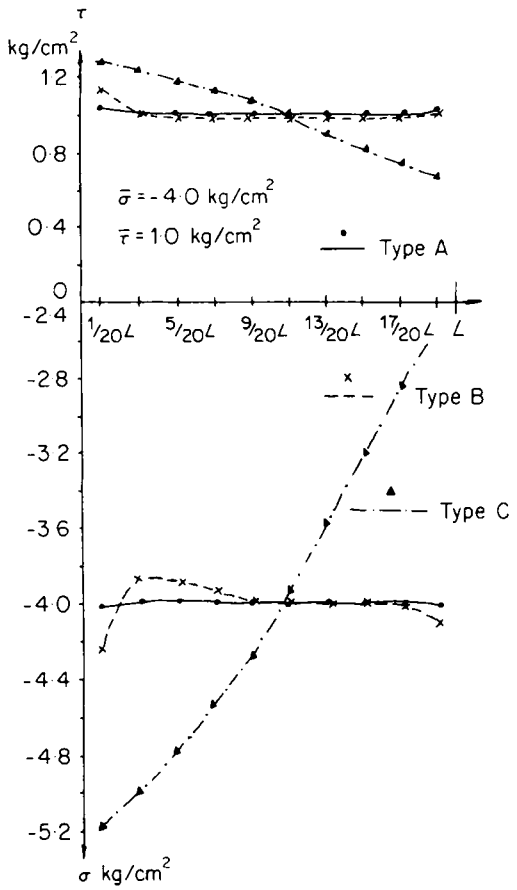

Figure 11. The stress distribution of weak intercalation (refer to Figure 10(a))

It must be noted that with the variations in load, the stress distributions are also variable. Even so the following points from the above figures should be noticed.

(a) Except for the case of weak intercalation with Type A of testing, the distribution of τ and σ along the shearing surface is not uniform in all cases for different types of testing.

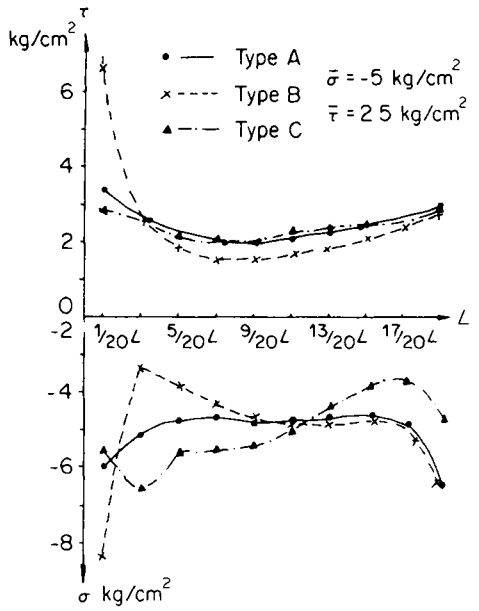

Figure 12. The stress distribution of the joint (refer to Figure 10(b))

(b) The distributions of stresses along the shearing surface in different cases of combination of joint, weak intercalation and rock using Type A of testing will be more uniform than those using Types B and C of testing.

(c) If the drop of the τ–U curve is evident, the results of calculations to simulate the same specimen will be different from each other, using the different types of testing. What is shown in

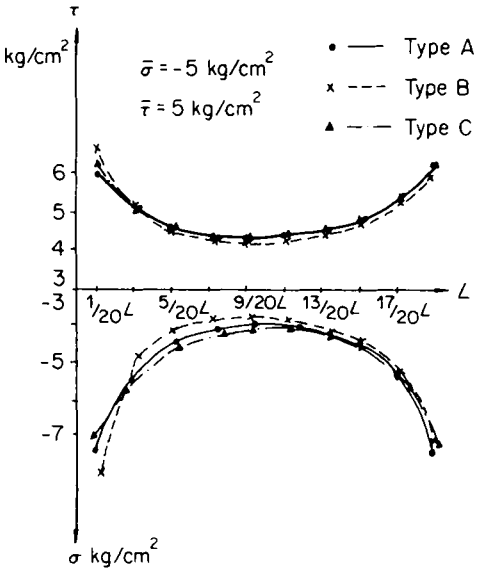

Figure 13. The stress distribution of the cemented surface (refer to Figure 10(c))

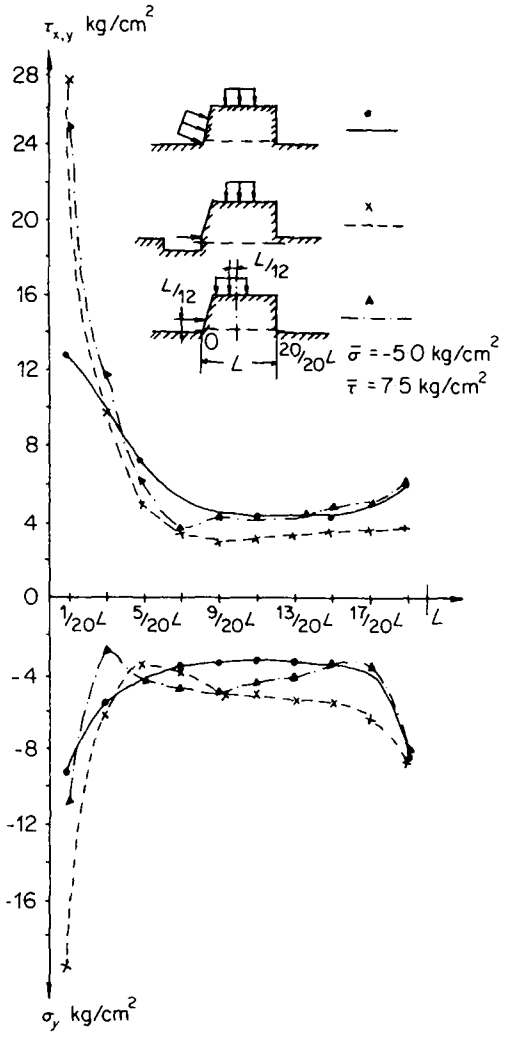

Figure 14. The stress distribution along the shearing surface of the rock mass specimen (refer to Figure 10(d))

Figure 15 are the calculated shear strengths for the cases described in Figures 10(b) and 10(c). It is seen that owing to the non-uniform distribution of stresses during testing and the drop of the τ–U curve, the shear strength obtained from the *in-situ* shear test, the results of which are calculated according to the concept of average amount of stresses along the shearing surface, is always less than the real shear strength on account of the uniform stress distributions.

(d) When there is not an evident drop of the τ–U curve, say, the case shown in Figure 10(a) (the properties of J_1 are the same as in Figure 5) the shear strengths obtained from different types of testing are quite coincident (Figure 16).

(e) In terms of not only the stress distribution but also the reliability of shear strength, the Type A is the best of the different types of testing in the four cases indicated in Figure 10.

It seems groundless that the stress distribution on the shearing surface is most uniform if Type B of testing is used.

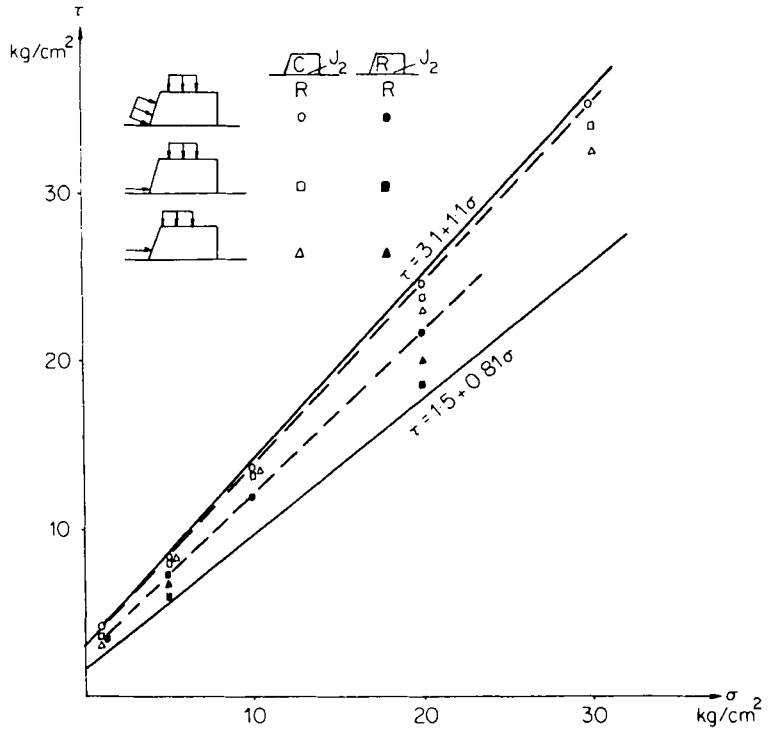

Figure 15. The results obtained from computation and the shear strength used in the calculation

ROCK SLOPE ANALYSIS

The analysis of the stress distribution and stability of the rock slope of an open pit mine has been made using the finite element method. The height of the slope is 225 m and the rock is marble. Some faults and weak bedding planes, which are simulated and described in calculations by the joint elements and the prementioned method of non-linear analysis, are given in the profile of

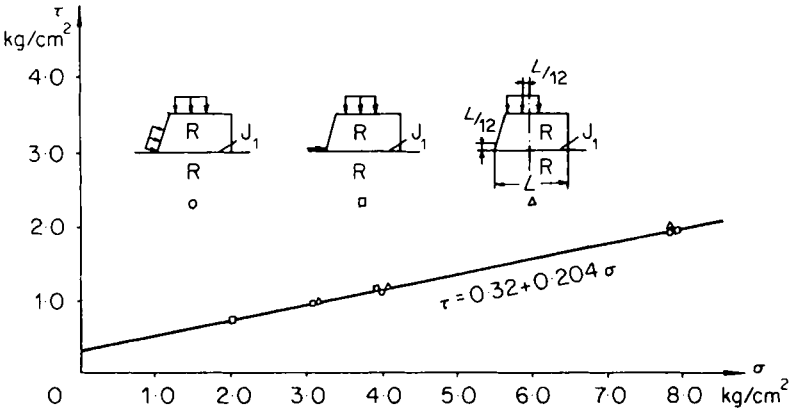

Figure 16. Relationship between the shear strength of weak intercalation and the types of testing

the slope (Figure 17(a)). Linear triangular elements have been employed for the rocks, and the failures of rock by tension and by shear and non-linear analysis have been considered.

The surface of ground water of the rock slope and the inversion of strata are also shown in profile (Figure 17(a)). In the body of the slope where the inversion of strata occurs, the integrity of the rock becomes somewhat bad, so the Young's modulus E (100,000 kg/cm^2) is lower than the E of intact rock (250,000 kg/cm^2).

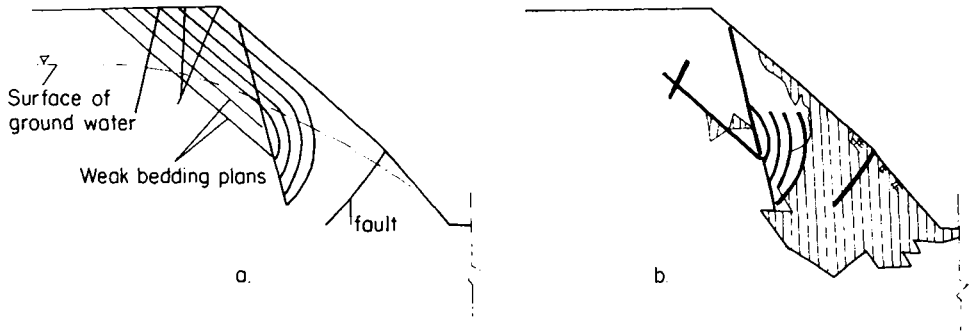

Figure 17. Finite element analysis of the rock slope

The type of the τ–U curve shown in Figure 4 (a) is employed to represent the fault and the weak bedding planes in the region where the inversion occurs. The mechanical properties are as follows: $C_p = C_r = 0$, $\tan \varphi_p = \tan \varphi_r = 0{\cdot}5$, $[\sigma_T] = 0$, $k_{s0} = 0$, $\alpha = 11{\cdot}7$ kg/cm^3 ($k_{s1} = k_{s2} = k_{s3}$, $m = 1$), $k_{n1} = k_{n2} = 700$ kg/cm^3, $k_{n3} = 0$.

The type of the τ–U curve shown in Figure 4(c) is employed to represent the weak bedding planes in other regions, C_p of which is 2·5 kg/cm^2, $\tan \varphi_p = 0{\cdot}532$, $C_r = 0$, $\tan \varphi_r = 0{\cdot}5$, $[\sigma_T] = 1{\cdot}0$ kg/cm^2.

For the case of $k_{s1} : k_{s0} = 40{\cdot}0$ kg/cm^3, $\alpha = 11{\cdot}7$ kg/cm^3 ($m = 1$). For the case of $k_{s3} : k_{s0} = 0$, $\alpha = 11.7$ kg/cm^3. $k_{n1} = k_{n2} = 700$ kg/cm^3.

Two basic variants have been considered, for one of which only body weight and the influence of ground water have been taken into account. The nodal forces due to the ground water are also calculated by the finite element method, and the calculations are carried out simultaneously with the whole process of analysis. For another variant, besides the prementioned factors, the influence of intial stresses which are due to geotectonic stress is also considered.

The calculated results of the first variant are given in Figure 17(b). It shows that some parts of bedding planes are subjected to shear failure, and in the location of the inversion of bedding planes the failure is more serious. The shear-sliding of some faults occurs. These bedding planes and faults are indicated in Figure 17(b) by bold lines. The yielding regions of the rock mass are represented by cross lines in the figure. In local regions failure by tension appears. Referring to the geotectonic stress data of the *in-situ* practical measurement in a deep borehole using the stress release method, the horizontal stress at the depth of 100 m is about 100 kg/cm^2, which is taken into account in the second variant in calculation.

The results of calculation of the second variant are very different and the stability of the rock slope in this case is much worse than that of the first variant. This explains that the influence of the geotectonic stress upon the stability analysis of a rock slope must be considered in detail.

THE CALCULATION TO SIMULATE *IN-SITU* ROCK RESISTING BODIES

According to the requirement for investigating the stability of a concrete dam on a soft rock foundation (argillaceous siltstone) *in-situ* compression tests on rock resisting bodies, the length of which exceeds 10 m, have been performed in order to obtain the ultimate load capacity and knowledge about the failure process along the weak planes of such soft rock. There is a mud layer of weak intercalation between the rock specimens and foundation rock. Its mechanical properties are the same as shown in Figure 5. Besides, there are other three weak bedding planes existing in specimens of resisting bodies and parallel to the mudded layer. The computation to simulate the *in-situ* tests has been made and the schematic diagram is seen in Figure 18.

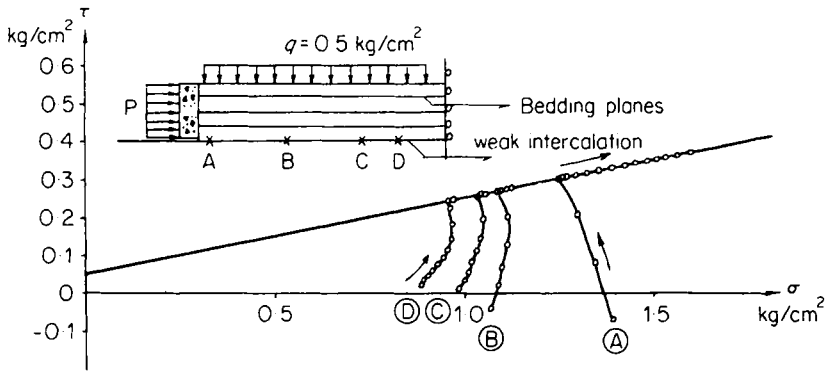

Figure 18. Computation to simulate the resisting body

The vertical load q for one of specimens is 0·5 kg/cm^2. It is observed *in situ* that the intensity of the horizontal thrust p is less than 2 kg/cm^2 when the failure of the weak plane occurs, and the value obtained by computation is 1 kg/cm^2.

The measured values of the intensity of the horizontal thrust p fall in the range of 4 to 6 kg/cm^2, and the result of calculation is 4·7 kg/cm^2. There is not a vertical load on another specimen. The measured values of p, when the mud layer began with failure and the failure occurred along the whole surface, are also quite in compliance with the calculated results. The values of stresses in four places on the weak planes obtained by calculation are given in Figure 18 when $q = 0{\cdot}5$ kg/cm^2 and p is increased from 0 to 5 kg/cm^2 (in 15 steps).

It is seen that the distribution of τ and σ is not uniform. The τ at the end close to the thrust increases rapidly with the increase of p. At the other end the τ of the mud layer increases slowly. It means that there is a gradually spreading process in the failure of the thin mud layer following the inerease in p, and this is also coincident with the *in-situ* measured data.

THE SHEAR STRENGTH CHARACTERISTIC LINE OF WAVE-LIKE WEAK INTERCALATION

The condition of wave-like weak intercalations may often be encountered. In many cases the length of every 'wave' is far longer than that of the specimen practically adopted in an *in-situ* shear test. Deere *et al.*[9] have pointed out that in such a case (Figure 19) the results of tests of the 6-in or 3-ft specimens may be comparable, but the entire surface could still exhibit a shear strength much different from the results of test. In order to simulate these cases the compu-

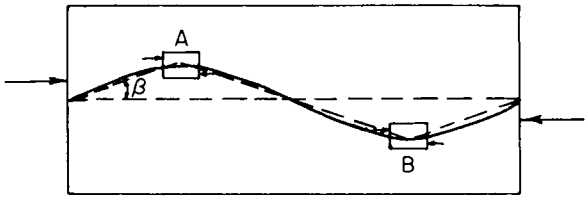

Figure 19. Simplification of wave-like weak plane

tations are performed with a simplification of wave-like form to a gentle saw-toothed plane, the dip angle β of which is equal to 5°, 10° or 15° respectively in different variants. The mechanical properties of the weak plane are the same as the properties of the weak intercalation shown in Figure 5. Figure 20 shows the shear strength line of the saw-toothed plane and the shear strength line of the weak intercalation having a flat form, which is represented by letter A in the figure. And hence it may be noted as follows:

(a) the shear strength of the saw-toothed weak plane is higher than that of the weak plane having a flat form;

(b) the larger the β, the more evident the increase in shear strength is, and a non-linear relation exists between β and the shear strength.

(c) The shear strength line of the saw-toothed and soft weak plane exhibits a bilinear type. The dip angle at the initial stage is comparatively steep and is about $(\varphi_r + \beta)$. When σ is larger the strength line is higher but approximately parallel to line A.

The results of tests to simulate the unfilled saw-toothed plane having a steeper dip angle, performed by Patton[10], showed that the strength line also exhibits the bilinear character. It is seen that the form of strength line is similar to the prementioned results of calculation, but owing to the different conditions and research objects the failure mechanisms are not completely the same.

What we have studied are the filled, soft, comparatively thick intercalation planes. Hence the portion having an increase in dip angle on the shear line means that when failure takes place the opening out occurs on one side of the saw tooth. However, when failure occurs in that portion of the line parallel to line A, the whole saw-toothed weak plane still exists in the state of compaction. No opening out takes place. The condition of the rock sheared off along the shearing surface does not appear. This is in good coincidence with the description of the failure mechanisms obtained from simulation tests performed when the filling in the joints is comparatively soft and thick, noted by some references.

This portion of the shear strength line is higher than line A and parallel to it, just as the value of C in Coulomb's criterion is increased and becomes $C(\beta, S)$. Therefore it can be regarded as a

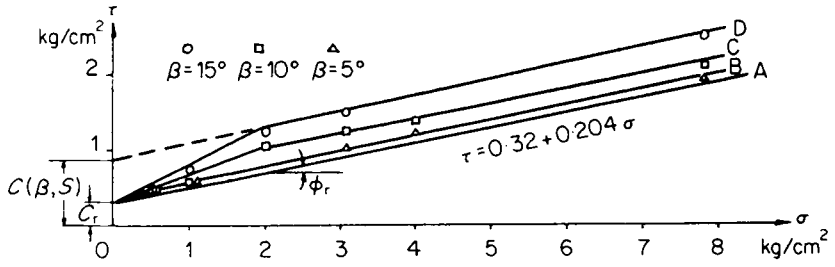

Figure 20. Shear strength of the saw-toothed planes

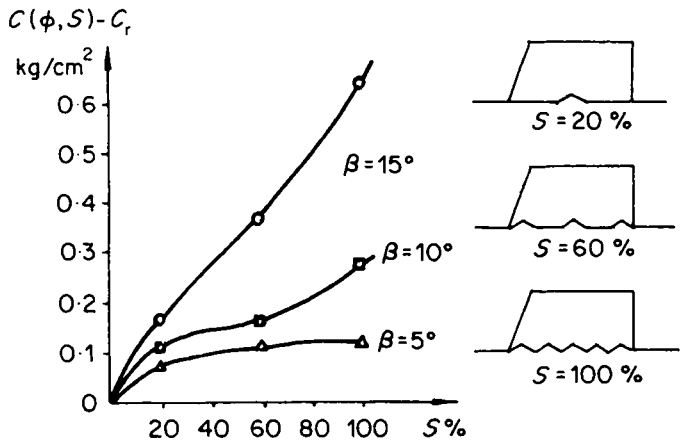

Figure 21. Influence of S upon the shear strength

comprehensive effect of the cohesion of the weak plane itself in the flat form and the influence of the wave-like form of the weak plane. Certainly $C(\beta, S)$ is dependent not only on the amount of dip angle β but also on S, which is the percentage of the saw-toothed surface to the whole shearing surface. What is shown in Figure 21 is the relationship between C' and β, C_r where $C' = C(\beta, S) - C_r$.

CONCLUSION

The model to simulate the non-linear properties of joint elements and method of non-linear analysis based on the incremental procedure are given.

One of the advantages of the proposed method is that it is adaptable to the different types of τ–U curve and simulates conveniently the complicated process of loading–unloading-reloading.

The opening and reclosing of the joint element can also be taken into account in calculation. The proposed method has been used in rock engineering problems of several types, and the results obtained from computation are quite satisfactory.

About the different types of *in-situ* shear testing, the simulation calculation shows the stress distribution on the shear surface, generally speaking, is not uniform, but Type A of testing shown in Figure 11 is the best of the three types, owing to the comparatively uniform distribution of stresses in this case.

The shear strength line of the wave-like weak plane exhibits a bilinear form and is higher than the shear strength line of the weak plane having a flat form.

It is seen in rock slope analysis that the influence of geotectonic stress upon the slope stability should not be neglected.

The computation to simulate the *in-situ* test of rock resisting bodies exhibits the progressing failure of weak intercalations between the specimen and rock foundation with the increase of horizontal thrust.

NOTATION

C_A = cohesion of the shear strength line A of the joint
C_p = cohesion of the peak shear strength of the joint
C_r = cohesion of the residual shear strength of the joint

$[C]$ = matrix for the elastic properties of the joint
$[C_{ep}]$ = matrix for the elastic–plastic properties of the joint
E = Young's modulus of rock
F = yielding surface
G = plastic potential surface
k_n = unit normal stiffness of the joint
k_s = unit shear stiffness of the joint
k_{nn} = one of the four components of $[C_{ep}]$
k_{ns} = one of the four components of $[C_{ep}]$
k_{sn} = one of the four components of $[C_{ep}]$
k_{ss} = one of the four components of $[C_{ep}]$
p_a = atmospheric pressure
S = percentage of the saw-tooth surface to the whole shearing surface
U = relative shear displacement of the joint
V = relative normal displacement of the joint
$\bar{V}$ = parameter used to identify the state of the joint element
V_{max} = parameter about the ultimate relative deformation due to compression
β = saw-tooth's dip angle
ν = Poisson's ratio of rock
σ = normal stress of the joint element
σ' = residual normal stress of the joint element
$\bar{\sigma}$ = average normal stress of the shearing surface
$[\sigma_T]$ = tensile strength of the joint
τ = shear stress of the joint element
τ' = residual shear stress of the joint element
$\bar{\tau}$ = average shear stress of the shearing surface
φ_A = frictional angle of the shear strength line A of the joint
φ_p = frictional angle of the peak shear strength of the joint
φ_r = frictional angle of the residual shear strength of the joint

REFERENCES

1. R. E. Goodman, R. L. Taylor and T. L. Brekke, 'A model for the mechanics of jointed rock', *J. Soil Mech. Found. Div., Proc. Am. Soc. Civ. Eng.*, **94** (1968).
2. R. E. Goodman, 'The mechanical properties of joints', *Proc. 3rd Congress. Intl. Soc. for Rock Mech.*, Denver (1974).
3. R. E. Goodman, *Methods of Geological Engineering in Discontinuous Rocks*, West Publishing Co., Berkeley, 1976.
4. R. M. Clough and J. M. Duncan, 'Finite element analysis of retaining wall behaviour', *J. Soil Mech. Found. Div., Proc. Am. Soc. Civ. Eng.*, **97** (1971).
5. O. C. Zienkiewicz, B. Best, C. Bullage and K. G. Stagg, 'Analysis of nonlinear problems in rock mechanics with particular reference to jointed rock systems', *Proc. 2nd Congress, Intl. Soc. of Rock Mech.* Belgrade (1970).
6. J. Ghaboussi, E. Wilson and J. Isenberg, 'Finite element analysis for rock joints and interfaces', *J. Soil Mech. Found. Div., Proc. Am. Soc. Civ. Eng.*, **99** (1973).
7. R. M. Barker and F. Hatt, 'Joint effects in bedded formation roof control', *Proc. 14th Symposium on Rock Mech.* Pennsylvania (1972).
8. Ke Hsu-jun (Ge Xiurun), 'Non-linear analysis of the mechanical properties of joint and weak intercalation in rock', *Proc. 3rd Intl. Conf. on Numerical Methods in Geomechanics*, Aachen, **2** (1979).
9. D. R. Deere *et al.*, 'Design of surface and near surface construction in rock', *Proc. 8th Symposium on Rock Mech.* Minnesota (1966).
10. F. D. Patton, 'Multiple modes of shear failure in rock', *Proc. 1st Congress, Intl. Soc. of Rock Mech.* Lisbon (1966).